Journal of CO2 Utilization 68 (2023) 102356

Contents lists available at ScienceDirect

Journal of CO2 Utilization

journal homepage: www.elsevier.com/locate/jcou

Spinel ferrite catalysts for CO_2 reduction via reverse water gas shift reaction

J.C. Navarro [a,*], C. Hurtado [a], M. Gonzalez-Castaño [a], L.F. Bobadilla [a], S. Ivanova [a], F.L. Cumbrera [b], M.A. Centeno [a], J.A. Odriozola [a,c]

[a] Instituto de Ciencia de Materiales de Sevilla, Centro Mixto CSIC-Universidad de Sevilla, Avda. Américo Vespucio 49, 41092 Seville, Spain
[b] Departamento Física de la Materia Condensada, Universidad de Sevilla, 41080 Seville, Spain
[c] Department of Chemical and Process Engineering, University of Surrey, Guildford Surrey GU2 7XH, United Kingdom

ARTICLE INFO

Keywords:
Spinel
Ferrite
Cu
Ni
Oxygen vacancies
Raman
RWGS reaction

ABSTRACT

The production of CO via Reverse Water Gas Shift (RWGS) reaction is a suitable route for CO_2 valorization. In this study a series of modified spinels AB_2O_4 (A site = Ni, Zn and Cu and B site=Fe) are investigated as RWGS catalysts and their structure-to-function relationships derived from the changes on the A-site cation are rationalized. For all ferrite systems, the RWGS reaction the process main activity and selectivity is governed by the B-site cation, but the variations on the A-site metals determines catalysts' structural features and stability in the reaction. Among the catalyst series, superior RWGS performance displayed the ferrites modified with Cu and Ni associated to the greater oxygen vacancy population for those spinels enabled by the partial allocation on Fe^{3+} cations into the tetrahedral sites.

1. Introduction

The utilization of CO_2 as a renewable source for the production of commodities and fuels has become a primordial chemical route for the intended energetic transformation and concomitant implementation of Power to Gas (PtG) technologies [1]. In the last decade the transformation of CO_2 to CO and syngas mixtures has generated a renewed interest in Reverse Water Gas Shift reaction (RWGS) (Eq. 1).

$$CO_2 + H_2 = CO + H_2O \quad (1)$$

$$CO_2 + 4H_2 = CH_4 + 2H_2O \quad (2)$$

The reduction of CO_2 via RWGS is an endothermic process thermodynamically and kinetically favored at high temperatures. Operating at lower temperature should result in depleted yields since undesired side reactions like Water Gas Shift (WGS) and CO_2 methanation (Eq. 2) occurred. That is why the crucial task to maximize the CO production at relatively moderated reaction temperatures is the design of effective and selective RWGS catalysts. Among the different systems, the excellent performance-to-price ratio of the Fe based catalysts renders them very promising candidates to investigate and improve [2,3]. In fact, the high melting point and the redox character of Fe metal gives chief features for RWGS catalyst like optimal thermal stability and resilience against carbon deposits. A way to improve the performance of the RWGS catalysts is the combination of two transition metals into binary spinel oxides resulting in extremely convenient structures [4]. Compared to the simple mixture of metal oxides the spinel-like structures are often associated to narrower particle size distribution, optimal stoichiometric control and as a consequence greater active surface available for catalytic reaction [5]. Structurally, ferrites with general formula AFe_2O_4, with A any divalent cation, exhibit cubic structures with iron ions occupying octahedral sites and, A^{2+} cations occupying tetrahedral sites. The arrangement of the iron species into spinel network could vary along the octahedral holes (like in normal spinel structure) or might also fill partially some tetrahedral sites (inverse spinel structure). The structural and redox features of the doped-ferrites depend on the nature of the A-site cation and synthesis methods. In fact, A-site cation type and its relative occupancy among the tetrahedral and octahedral sites determines the spinel structure, the overall system properties and behavior [6]. Any variation on this distribution provokes a different occupation of the octahedral positions (ratio filled/empty), being affected in greater manner the distribution of the empty sites typically accumulated at solid's surface. With this in mind any change of the A- site would provoke important redistribution of the empty sites on the surface and as a consequence the reactive adsorption and surface catalytic reaction.

The Iron-chromia ferrite catalyst are well-known catalytic systems for the forward WGS reaction being the incorporation of Cr beneficial for the stability of the active magnetite phase. However, the behaviour of

* Correspondence to: King Abdullah University of Science and Technology, KAUST Catalysis Center (KCC), Thuwal 23955-6900, Saudi Arabia.
E-mail address: juancarlos.navarrodemiguel@kaust.edu.sa (J.C. Navarro).

https://doi.org/10.1016/j.jcou.2022.102356
Received 19 September 2022; Received in revised form 25 November 2022; Accepted 5 December 2022
Available online 22 December 2022

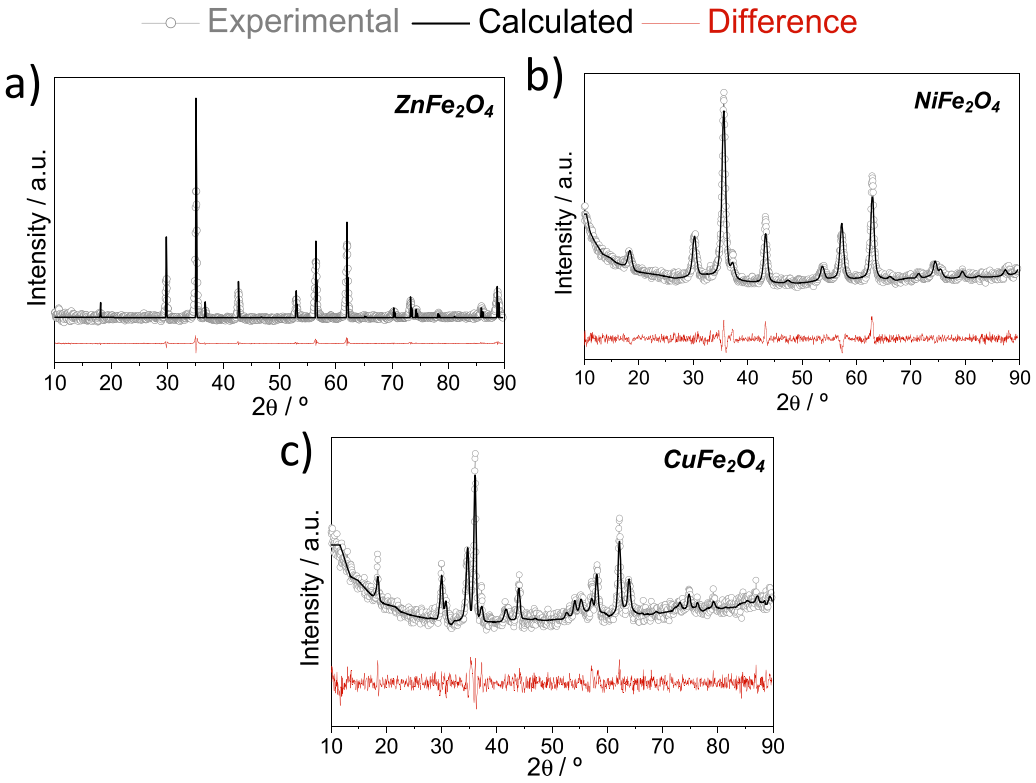

Fig. 1. Refined XRD patters of a) $ZnFe_2O_4$, b) $NiFe_2O_4$, and c) $CuFe_2O_4$ samples.

the ferrite catalysts in RWGS reaction and especially the influence of the A-site cations on the performance of the catalysts towards CO_2 reduction is far less studied. Nordhei et al. [7] investigated the reactivity of nanosized $CoFe_2O_4$, $NiFe_2O_4$ and $ZnFe_2O_4$ catalysts in CO_2 dissociation. They found an important influence of the A cation nature on system reducibility, M^{2+}/M^{3+} redox pair reversibility, and electronic properties thereby affecting the CO_2 dissociation abilities. Profiting the abilities of partially reduced spinels for dissociating CO_2 molecules, some works have investigated the performance of binary and ternary ferrites as oxygen carriers in low temperature chemical looping (CL) applications. Qiu et al. [8] investigated a series of AFe_2O_4 (A = Co, Cu, Ni) catalysts for CL-RWGS reaction and concluded that the catalytic performances of the systems depends on their redox behaviour (Co better than Cu). On the opposite Xian et al. [9] found Cu ferrite system the one with better redox and catalytic behaviour. The different synthesis methods and reaction conditions employed in these studies might account for such discrepant outcomes. To the best of our knowledge, the impact of A-site cations in ferrite spinel catalysts has not been systematically investigated under RWGS atmospheres. Therefore, a series of AFe_2O_4 catalysts with A = Ni, Cu, and Zn are proposed for a detailed study of the A-site cations role on ferrites structure, redox properties and performance in the RWGS reaction.

2. Experimental

2.1. Catalyst synthesis

The catalysts ($NiFe_2O_4$, $CuFe_2O_4$ and $ZnFe_2O_4$) were prepared via co-precipitation method. According to the methodology proposed in earlier works [10,11], the corresponding metal nitrates ($FeNO_3{\cdot}9\ H_2O$, Ni $(NO_3)_2{\cdot}6\ H_2O$, $Zn(NO_3)_2{\cdot}6\ H_2O$ and $Cu(NO_3)_2{\cdot}3\ H_2O$) were employed. The adequate amounts of nitrate salts dissolved and stirred at 70 °C during 24 h are used as starting solution. Then, NaOH (2 M) and $CaCO_3$ (0.5 M) were slowly added until pH = 10 was reached. The obtained precipitate was thoroughly washed with deionized water, dried overnight and calcined at 650 °C (5 °C/min heating rate) for 12 h.

2.2. Characterization techniques

The X-Ray Diffraction analysis was carried out on a X´Pert Pro PANalytical diffractometer at room temperature using Cu Kα radiation (40 mA, 45 kV), in the 2Θ range of 10–90º, and a position sensitive detector with step size of 0.05º and step time of 300 s. Raman spectra were obtained in a dispersive Horiba Jobin Yvon LabRam HR800 Confocal Raman Microscope using a green laser (λ = 532.14 nm), working at 5 mV power and using a 600 grooves/mm grating. The microscope used a 50x objective with a confocal pinhole of 1000 μm.

The temperature-programmed reduction (H_2-TPR) was carried out in a TPR equipment (PID Eng&Tech®). For this, the catalyst (50 mg) was loaded into a U-shape quartz reactor, and it was cleaned with an Ar flow (50 mL/min) for 20 min at room temperature. Then, a total flow of 50 mL/min of H_2 5 vol% in Ar was applied over the catalyst while the temperature was raised from room temperature to 900ºC (10ºC/min). A cold trap was set prior to the thermal conductivity detector (TCD) during the reduction processes. TCD signals and temperature were reactorded in each analysis with the program Process@ developed by PID Eng&Tech®.

2.3. Catalytic activity measurements

The catalytic activity measurements were carried out in a Microactivity PID Eng&Tech® equipment using a 9 mm internal diameter AISI316 stainless steel tubular reactor (Autoclave Engineers®). The catalysts were sieved to a particle size $100 < \phi < 200$ μm, and diluted with SiC VWR Prolabo® (125 μm) to a bed volume of 0.5 cm^3. The system was heated at 400ºC in N_2, subsequently replaced with the reaction mixture (60 mL·min^{-1} H_2, 15 mL·min^{-1} CO_2 ratio and N_2 until 100 mL·min^{-1}). The catalytic behaviour was evaluated at every 50ºC from 400º to 700ºC (up), and from 700º to 400ºC (down) for all studie samples.

Table 1
Refined parameters for the prepared catalysts.

Sample	Lattice parameter, (Å)	Degree of inversion (i)	Agreement factors, X^2
ZnFe$_2$O$_4$	a = 8.4603	0.152	1.34
NiFe$_2$O$_4$	a= 5.9053 c= 8.3646	0.998	1.12
CuFe$_2$O$_4$	a= 5.8245 c= 8.6736	0.952	1.05

The reactants and products were analysed using on-line gas chromatography (GC) using a Varian micro GC 4900 instrument with two thermal conductivity detector (TCD) channels, one equipped with Porapaq-Q and other with Molecular Sieve 5 A column. The CO_2 at the reactor outlet was also recorded with a Vaisala® detector CARBOCAP GMT220. CO_2 conversion (X_{CO2}), yield to CH_4 and CO, and carbon balance were estimated using Eqs. (3–6) respectively.

$$X_{CO_2}(\%) = \frac{(F_{CO_2in} - F_{CO_2out})}{F_{CO_2in}} x100 \quad (3)$$

$$Y_{CH_4}(\%) = \frac{F_{CH_4out}}{F_{CO_2in}} x100 \quad (4)$$

$$Y_{CO}(\%) = \frac{F_{COout}}{F_{CO_2in}} x100 \quad (5)$$

$$C = \frac{F_{CO_2out} + F_{COout} + F_{CH_4out}}{F_{CO_2in}} x100 \quad (6)$$

3. Results and discussions

Fig. 1 summarizes the XRD data obtained for the as-prepared ferrites including experimental diffractograms, their Rietveld refinement and the difference between both sets of data. The ***ZnFe$_2$O$_4$*** sample shows the characteristic diffractions of the cubic spinel polymorph (Fd-3 m (227), JCPDS 00-001-1109) while tetragonal spinel structures (141/and (141)) were identified for ***NiFe$_2$O$_4$*** (JCPDS 00-086-2267) and ***CuFe$_2$O$_4$*** (JCPDS 00-034-0425) systems. An optimal agreement was found between the experimental data and Rietveld refinement for all ferrite structures. What is more, the Rietveld analysis allowed the estimation of the site occupation and the categorization of the prepared ferrites. For ***ZnFe$_2$O$_4$***, the performed adjustment shows an X^2 value of 1.34, distortion parameter (u) of 0.258 and degree of inversion (i) equal to 0.152, corresponding to a normal (direct) spinel structure (Table 1). The distances between the Fe_1 atoms in octahedral positions to Zn_2 and Fe_2 atoms in tetrahedral positions are 3.5085 Å, while the distances to Zn_1 and Fe_1 atoms in octahedral sites is 3.6645 Å. However, that distance is quite different for Fe_2 and Zn_2 (2.9921 Å) indicating a distortion of the cubic structure. Nevertheless, a full tetragonalization of the structure is observed for ***NiFe$_2$O$_4$*** and ***CuFe$_2$O$_4$*** samples with an important degree of inversion, 0.998 and 0.952 respectively, pointing directly to a constitution of inverse spinel.

Raman spectroscopy is an effective technique for characterizing the structure of metal oxides and enables the identification and quantification of point defects like oxygen vacancies. Fig. 2 presents the deconvoluted Raman spectra of the prepared catalysts. Five optical Raman-active modes $A_{1g} + E_g + 3\,F_{2g}$ are reported for the spinel structures The A_{1g} mode at around 600 cm^{-1} is associated to the symmetric stretch of the tetrahedral M-O bonds while the E_g and F^3_{1g} Raman-modes at lower wavelengths are attributed to symmetric and antisymmetric M-O bending in octahedral sites. The remaining F^1_{1g} and F^2_{1g} bands are attributed to the translation of the MO_4 tetrahedral units and to the asymmetric stretch of the M-O bonds, correspondingly [12]. For all synthetized ferrites, the observed Raman bands were associated to a normal first-order Raman scattering due to internal lattice vibrations of the tetrahedral and octahedral sites for cubic (***ZnFe$_2$O$_4$***), and tetragonal spinels (***NiFe$_2$O$_4$*** and ***CuFe$_2$O$_4$***).

The relative variations of position and intensity of the Raman bands among the series could be related to the nature of the A-site cations [13]. A shift of the A_{1g} band is observed for $NiFe_2O_4$/$CuFe_2O_4$ tetragonal phases and $ZnFe_2O_4$ cubic ferrite and could be assigned to the differences in cation distribution in the tetrahedral and octahedral sites. The inversion of the spinel ($ZnFe_2O_4$ vs. $CuFe_2O_4$ and $NiFe_2O_4$) results in higher intensity of the F^2_{2g} band and red shifted A_{1g} mode. On the other

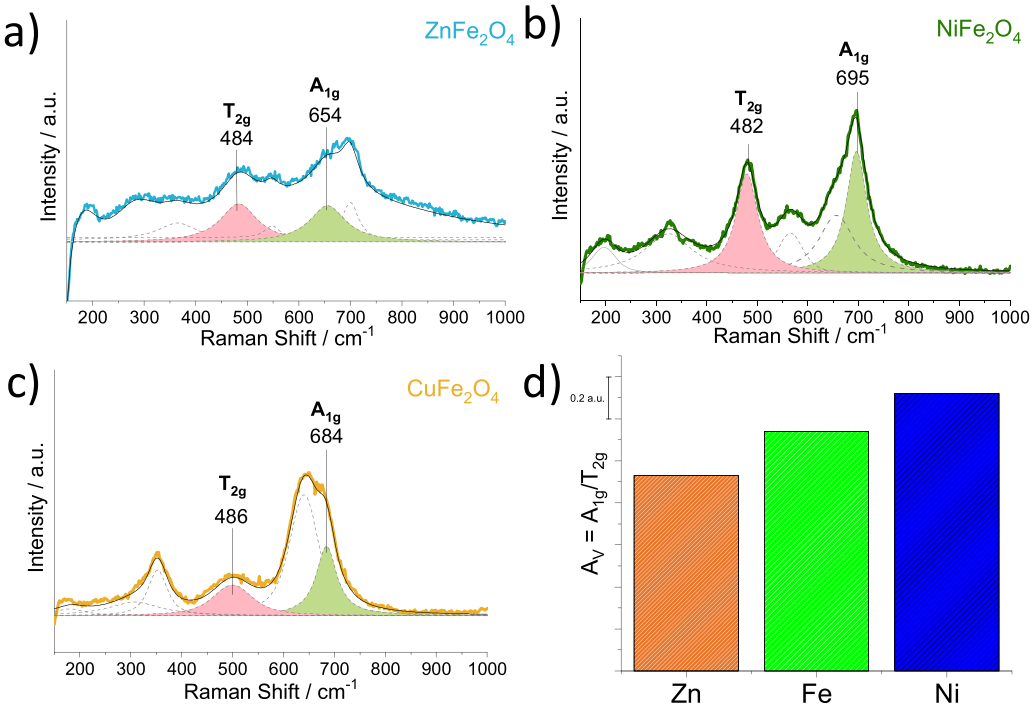

Fig. 2. Deconvoluted Raman spectra of: a) $ZnFe_2O_4$, b) $NiFe_2O_4$, c) $CuFe_2O_4$, and d) Intensity ratio A_V (A_{1g}/F^2_{2g}) estimated for the ferrite systems.

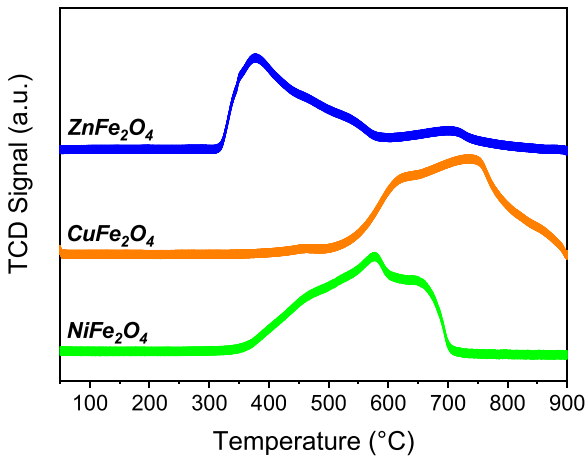

Fig. 3. H_2-TPR of the synthetized samples.

hand, the relative octahedral/tetrahedral sites distribution is also associated to the generation of point defects. It is argued that higher cationic occupancy of the tetrahedral sites provokes a contraction of the octahedral sites, resulting in Fe^{+3} sites strain [3]. In other words, greater amount of cations in tetrahedral sites provokes octahedral holes shrinking and facilitates oxygen vacancies formation. What is more, as $F2_{2g}$ and $A1_g$ bands are associated to A-cations in tetrahedral and octahedral sites respectively, a qualitative estimation of the oxygen vacancies concentration can be derived from the intensity ratio $A_V = A1_g/F2_{2g}$ [14,15]. The A_V values estimated for the ferrite samples are plotted in Fig. 2D and an oxygen vacancies concentration increase is found from Zn to Cu spinel. This observation is confirmed also by our XRD data and the higher amount of A-cations found in tetrahedral positions for Cu and Ni spinel structures in comparison to that of Zn. The driving force for A-site cations tetrahedral positions occupation is usually related to cations' oxygen affinity (cations nature) and their ability to for a sp^3 coordination [16,17]. We can conclude that the oxygen vacancy concentration (i.e. the $A_V = A1_g/F2_{2g}$ intensity ratio) increases as the oxygen affinity of the A-site cation decreases, as it enables the allocation of the iron ions into tetrahedral positions [18].

The reducibility of the samples was evaluated by H_2-TPR (Fig. 3). All ferrites exhibit reduction profiles of three reduction steps being the first one associated to the breakdown of the ferrite structure. For the $CuFe_2O_4$ and $NiFe_2O_4$ samples, the lower reduction zone could be associated to the simultaneous reduction of Cu^{2+} or Ni^{2+} cations and the decomposition of the spinel structure to Fe_2O_3/Fe_3O_4 mixture [19]. On the other hand the two reduction steps at higher temperatures are characteristic for iron species reduction i.e. $Fe_3O_4 \rightarrow FeO \rightarrow Fe^0$ [20]. As for the $ZnFe_2O_4$ sample, the appearance of metallic Zn seems unlikely. Even though, a highly defective metal oxide might be expected [21]. Hence, the three reduction steps discerned for the $ZnFe_2O_4$ sample are mostly associated to the spinel decomposition and sequential reduction of iron species [22,23]. The reducibility of the ferrites is obviously influenced by the incorporation of second metal and the overall reduction behaviour is modulated by the nature of this modifying cation [19,22]. Combining DFT and experimental XPS/TPR techniques, Liu et al. [22] claimed that the greater amounts of Fe^{2+} species distributed in highly defective ferrites affect negatively the reducibility of the ferrites. Accordingly, one could state that higher the oxygen vacancies concentration higher the reduction temperature. Indeed, the reduction temperature is inversely proportional to oxygen vacancies concentration found by Raman spectroscopy, following the trend: $ZnFe_2O_4 < NiFe_2O_4 < CuFe_2O_4$.

3.1. Catalytic activity

The catalytic activity was measured in two cycles: i) heating or

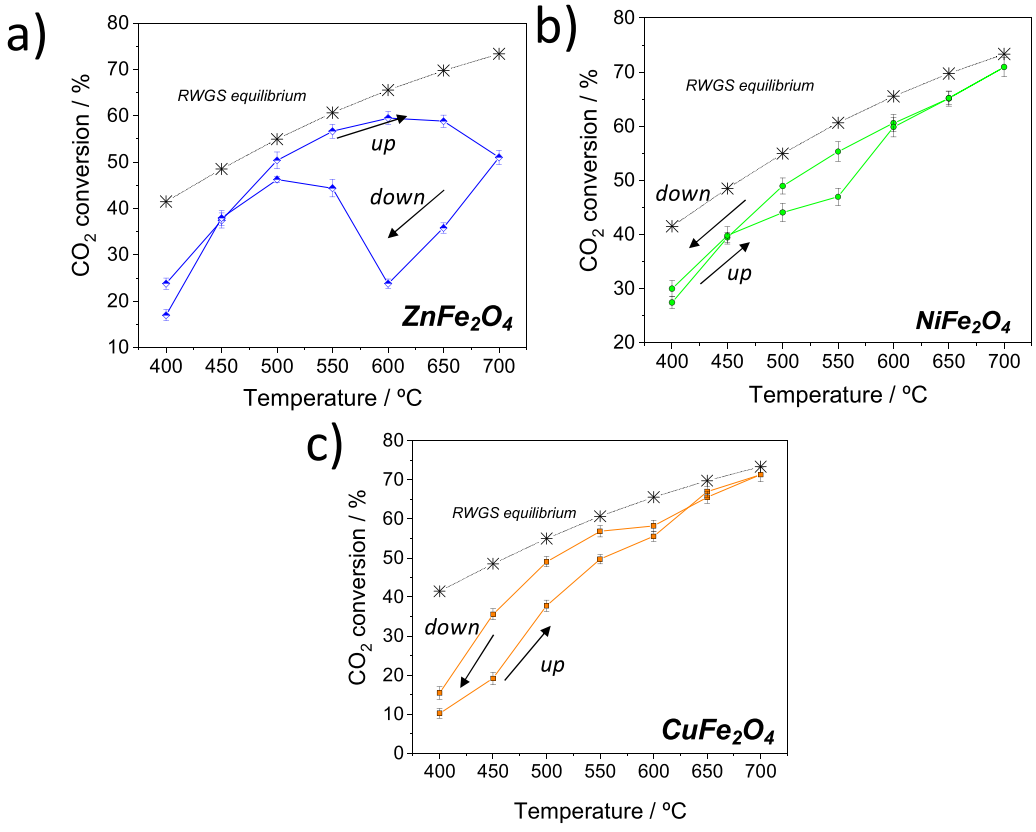

Fig. 4. CO_2 conversion values exhibited by the samples at 60 $L \cdot g^{-1} \cdot h^{-1}$ and $H_2:CO_2 = 4$.

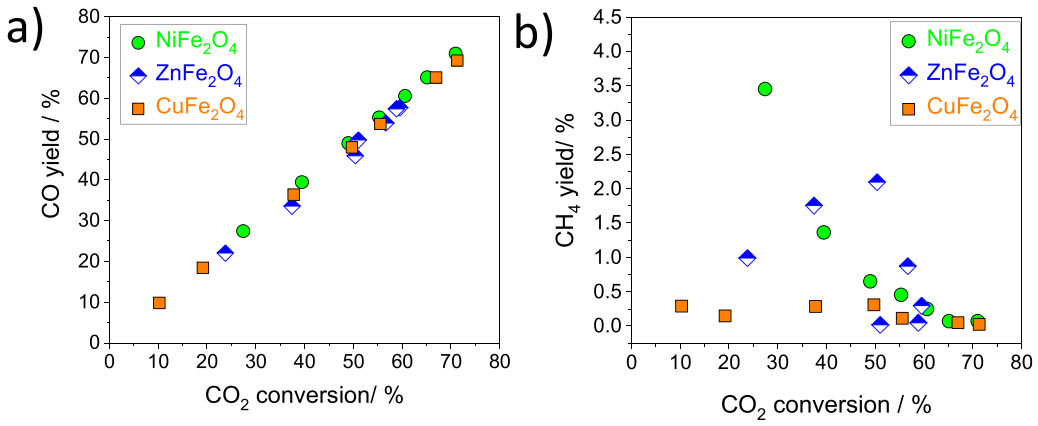

Fig. 5. a) CO yield and b) CH_4 yield vs. CO_2 conversion for the catalysts.

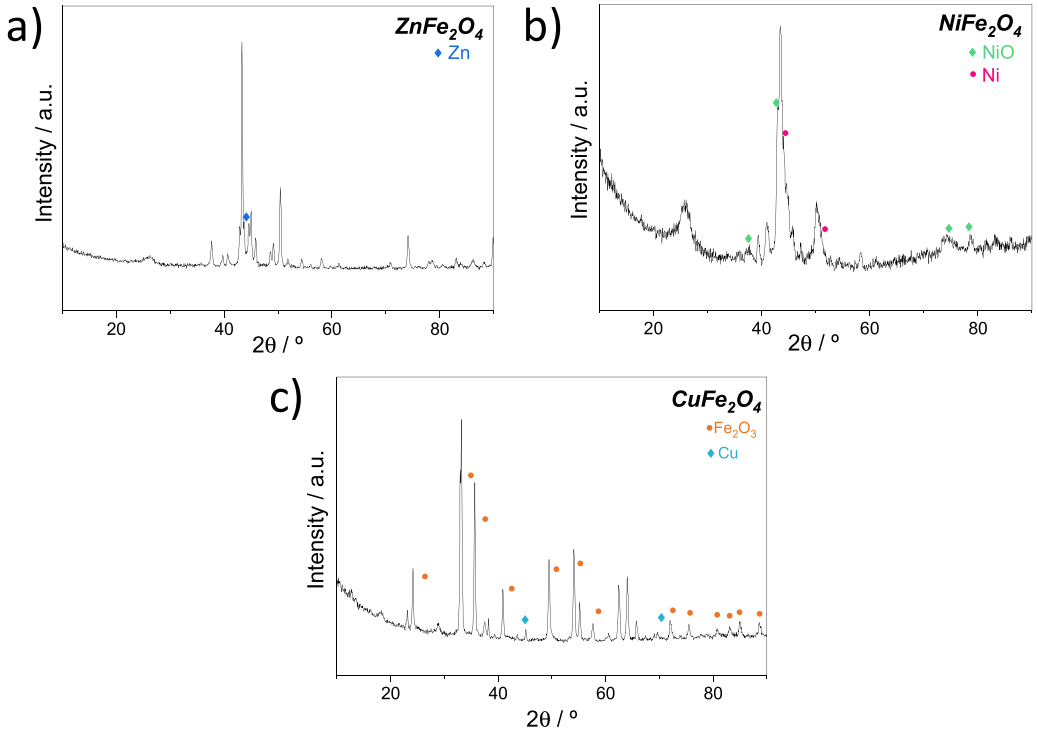

Fig. 6. XRD pattern after reaction of: a) $ZnFe_2O_4$, b) $NiFe_2O_4$, c) $CuFe_2O_4$.

increasing the temperature until 700ºC stepwise, and ii) cooling, decrease of the temperature to 400ºC. Fig. 4 summarizes the RWGS performance of the samples at H_2:CO_2 ratios of 4 and weight gas velocity of 60 $L{\cdot}g^{-1}{\cdot}h^{-1}$. The carbon balance for all the cases is 99 ± 2 %. $NiFe_2O_4$ sample shows the best performance attaining conversion values at lower temperatures and stability. The heating/cooling cycles repeat suggest that the catalyst does not suffer any important modification under reaction conditions. On the contrary, greater conversions are attained by $CuFe_2O_4$ sample during the cooling cycle and could be related to better reducibility and dispersion of metallic copper after one heating cycle. As for the $ZnFe_2O_4$ sample, deactivation is observed even in the heating cycle (temperature above 600ºC) suggesting the more probably a decrease in the availability of reactive surface. Fig. 5 shows the obtained CH_4 and CO yields as a function of the CO_2 conversion values. The overall CO production rate increases with the temperature and all samples present high selectivity to CO. The presence of Ni and Zn results in some minor CH_4 generation in the lower temperature range.

RWGS reaction rules out under two principal pathways: redox and associative. For the associative mechanism, intermediates like carbonates, carboxyls and formates are constituted which then react with dissociated hydrogen species afterwards to release CO and H_2. As for the redox mechanism, firstly, the reduction of the catalyst surface by H_2 species occurs followed by the reduction of the adsorbed CO_2 to CO. The later mechanism is often argued for Fe catalyst at high temperature [23] which is greatly promoted by the presence of oxygen vacancies, although they promote also the associative pathway. As seen above, the nature of the A-site in the prepared ferrite catalysts affects the cationic occupancy and distribution of surface oxygen vacancies. Although, the observed catalyst behavior suggests CO_2 conversion pathway regulated by the B site cation (reaching the equilibrium in all cases in the 400–600 ºC range) its distribution and conditioning (activation/deactivation) depends on the A-site cation. That is why, an important selectivity to CO is observed for the series with minor CH_4 fractions produced at low temperatures in the presence of metal with high hydrogenation tendencies, like Ni [21]. The presence of Zn does not seem to influence the Fe-sites activity, while Ni and Cu affect either the hydrogenation activity

of the catalyst (to CH_4 at low temperatures for Ni) or the iron species reduction, distribution and stability in the case of Cu. Thus, better catalytic performances and stabilities at higher temperatures are observed for $NiFe_2O_4$ and $CuFe_2O_4$, both inverse spinel ferrites with great oxygen vacancies concentrations.

The XRD analysis of the spent catalysts (Fig. 6) shows important changes within the samples. The spinel structure is hardly detectable and a mixture of oxides and metals appear. Cu spinel converts in a metallic copper supported on well crystalline iron (III) oxide. The same is found for the Zn spinel although the appearance of the Fe_2O_3 is not that evident due more probably to the particle size decrease of the latter. The same can be suspected for the Ni spinel where the XRD is rulled by the appearance of NiO and Ni on less crystalline Fe(III) oxide phases (higher noise to signal ratio found for this sample). One can conclude that the Cu presence induces Fe (III) oxide crystallization and generating rapidly the active phases for the reaction. On the contrary the appearance of the metallic zinc decreases the number of active sites (being this metal inactive in the reaction) confirmed by the decrease of activity in the "down" cycle.

4. Conclusions

In this work, a series of spinel ferrites AB_2O_4 (A = Ni, Zn and Cu; B= Fe) are prepared, characterized and tested for the RWGS reaction. Under CO_2/H_2 atmosphere, the dominant CO_2 conversion pathway for all ferrite catalysts implies the B-site cation and showing an important CO selectivity above 500ºC. On the other hand, the A-site cation seems to govern the process selectivity at lower temperatures. More importantly, the A-site cation nature affects the overall catalysts' structure and reduction behaviour helping in this way to condition the active iron sites and to achieve an important surface distribution and to prevent any deactivation. Over $CuFe_2O_4$ and $NiFe_2O_4$ inverse spinels, the allocation on Fe^{3+} cations into the tetrahedral sites promotes the surface oxygen vacancy population and enabled an improved RWGS catalytic performances.

CRediT authorship contribution statement

J.C. Navarro, M. González-Castaño, S. Ivanova: Data curation, Writing – original draft. **C. Hurtado, M. González-Castaño, L.F. Bobadilla, M.A. Centeno, J.C. Navarro, F.L. Cumbrera:** Visualization, Investigation. **S. Ivanova, M.A. Centeno, J.A. Odriozola:** Supervision. **S. Ivanova, J.C. Navarro:** Writing – review & editing. **J.A. Odriozola, M.A. Centeno:** Funding acquisition.

Declaration of Competing Interest

The authors declare that they have no known competing financial interests or personal relationships that could have appeared to influence the work reported in this paper.

Data availability

Data will be made available on request.

Acknowledgements

Financial support for this work was obtained from Junta de Andalucía via grant US-1263288 and Spanish Ministerio de Ciencia e Innovación (MICIN) (Grant number RTI2018-096294-B-C33) all co-financed by FEDER funds from the European Union. Dr. González-Castaño acknowledges the Spanish Ministry of Universities and the European Union (Next Generation EU) for the excellence Maria Zambrano fellowship.

References

[1] M. González-Castaño, B. Dorneanu, H. Arellano-García, The reverse water gas shift reaction: a process systems engineering perspective, React. Chem. Eng. (2021), https://doi.org/10.1039/D0RE00478B.
[2] L. Pastor-Pérez, M. Shah, E. le Saché, T. Ramirez Reina, Improving Fe/Al_2O_3 catalysts for the reverse water-gas shift reaction: on the effect of Cs as Activity/selectivity promoter, Catalysts 8 (2018) 608, https://doi.org/10.3390/catal8120608.
[3] M. González-Castano, J.C. Navarro De Miguel, F. Sinha, S. Ghomsi Wabo, O. Klepel, H. Arellano-Garcia, Cu supported Fe-SiO_2nanocomposites for reverse water gas shift reaction, J. CO_2 Util. 46 (2021), 101493, https://doi.org/10.1016/j.jcou.2021.101493.
[4] D. Jeong, A. Jha, W. Jang, W. Han, H. Roh, Performance of spinel ferrite catalysts integrated with mesoporous Al 2 O 3 in the high temperature water – gas shift reaction, Chem. Eng. J. 265 (2015) 100–109, https://doi.org/10.1016/j.cej.2014.12.045.
[5] D. Jeong, W. Jang, J. Shim, H. Roh, ScienceDirect High temperature water e gas shift without pre- reduction over spinel ferrite catalysts synthesized by glycine assisted sol e gel combustion method, Int. J. Hydrog. Energy 41 (2016) 3870–3876, https://doi.org/10.1016/j.ijhydene.2016.01.024.
[6] M. González-Castaño, B. Dorneanu, H. Arellano-García, The reverse water gas shift reaction: a process systems engineering perspective, React. Chem. Eng. (2021), https://doi.org/10.1039/D0RE00478B.
[7] C. Nordhei, K. Mathisen, I. Bezverkhyy, D. Nicholson, Decomposition of carbon dioxide over the putative cubic spinel nanophase cobalt , nickel , and zinc ferrites, J. Phys. Chem. C (2008) 6531–6537.
[8] Y. Qiu, S. Zhang, D. Cui, M. Li, J. Zeng, D. Zeng, R. Xiao, Enhanced hydrogen production performance at intermediate temperatures through the synergistic effects of binary oxygen carriers, Appl. Energy 252 (2019), 113454, https://doi.org/10.1016/j.apenergy.2019.113454.
[9] G. Xian, S. Kong, Q. Li, G. Zhang, N. Zhou, H. Du, L. Niu, Synthesis of spinel ferrite MFe_2O_4 (M = Co, Cu, Mn, and Zn) for persulfate activation to remove aqueous organics: effects of M-Site metal and synthetic method, Front. Chem. 8 (2020) 1–11, https://doi.org/10.3389/fchem.2020.00177.
[10] S. Iftikhar, M.F. Warsi, S. Haider, S. Musaddiq, I. Shakir, M. Shahid, The impact of carbon nanotubes on the optical, electrical, and magnetic parameters of Ni^{2+} and Co^{2+} based spinel ferrites, Ceram. Int. 45 (2019) 21150–21161, https://doi.org/10.1016/j.ceramint.2019.07.092.
[11] M. J.A, A. P, N. S, K. J, P. F.H.I, J. J. prince, Flake-like $CuMn_2O_4$ nanoparticles synthesized via co-precipitation method for photocatalytic activity, Phys. B Condens. Matter 572 (2019) 117–124, https://doi.org/10.1016/j.physb.2019.07.047.
[12] Z.Z. Lazarević, C. Jovalekić, A. Milutinović, D. Sekulić, M. Slankamenac, M. Romčević, N.Z. Romčević, Study of nife 2O 4 and ZnFe 2O 4 spinel ferrites prepared by soft mechanochemical synthesis, Ferroelectrics 448 (2013) 1–11, https://doi.org/10.1080/00150193.2013.822257.
[13] D. Sharma, N. Khare, Tuning of optical bandgap and magnetization of $CoFe_2O_4$ thin films, Appl. Phys. Lett. 105 (2014) 1–5, https://doi.org/10.1063/1.4890863.
[14] L.S. Ferreira, T.R. Silva, V.D. Silva, T.A. Simões, A.J.M. Araújo, M.A. Morales, D. A. Macedo, Proteic sol-gel synthesis, structure and battery-type behavior of Fe-based spinels (MFe_2O_4, M = Cu, Co, Ni), Adv. Powder Technol. 31 (2020) 604–613, https://doi.org/10.1016/j.apt.2019.11.015.
[15] Y. Li, Y. Li, X. Xu, C. Ding, N. Chen, H. Ding, A. Lu, Structural disorder controlled oxygen vacancy and photocatalytic activity of spinel-type minerals: a case study of $ZnFe_2O_4$, Chem. Geol. 504 (2019) 276–287, https://doi.org/10.1016/j.chemgeo.2018.11.022.
[16] J. Philip, G. Gnanaprakash, G. Panneerselvam, M.P. Antony, T. Jayakumar, B. Raj, Effect of thermal annealing under vacuum on the crystal structure, size, and magnetic properties of $ZnFe_2O_4$ nanoparticles, J. Appl. Phys. (2007) *102*, https://doi.org/10.1063/1.2777168.
[17] S. Singh, N. Khare, Defects/strain influenced magnetic properties and inverse of surface spin canting effect in single domain $CoFe_2O_4$ nanoparticles, Appl. Surf. Sci. 364 (2016) 783–788, https://doi.org/10.1016/j.apsusc.2015.12.205.
[18] C. Trevisanut, O. Vozniuk, M. Mari, S.Y.A. Urrea, C. Lorentz, J.M.M. Millet, F. Cavani, The chemical-loop reforming of alcohols on spinel-type mixed oxides: comparing Ni, Co, and Fe ferrite vs magnetite performances, Top. Catal. 59 (2016) 1600–1613, https://doi.org/10.1007/s11244-016-0681-0.
[19] T.R. Reina, W. Xu, S. Ivanova, M.Á. Centeno, J. Hanson, J. a Rodriguez, J. A. Odriozola, In situ characterization of iron-promoted ceria-alumina gold catalysts during the water-gas shift reaction, Catal. Today 205 (2013) 41–48, https://doi.org/10.1016/j.cattod.2012.08.004.
[20] S. Saedy, M.A. Newton, M. Zabilskiy, J.H. Lee, F. Krumeich, M. Ranocchiari, J. van Bokhoven, Copper-zinc oxide interface as a methanol-selective structure in Cu-ZnO catalyst during catalytic hydrogenation of carbon dioxide to methanol, Catal. Sci. Technol. (2022), https://doi.org/10.1039/d2cy00224h.
[21] P.T.A. Santos, A.C.F.M. Costa, H.M.C. Andrade, Preparation of $NiFe_2O_4$ and $ZnFe_2O_4$ samples by combustion reaction and evaluation of performance in reaction water gas shift reaction - WGSR, Mater. Sci. Forum 727–728 (2012) 1290–1295, https://doi.org/10.4028/www.scientific.net/MSF.727-728.1290.
[22] M. Liang, W. Kang, K. Xie, Comparison of reduction behavior of Fe_2O_3, ZnO and $ZnFe_2O_4$ by TPR technique, J. Nat. Gas. Chem. 18 (2009) 110–113, https://doi.org/10.1016/S1003-9953(08)60073-0.
[23] J.A. Loiland, M.J. Wulfers, N.S. Marinkovic, R.F. Lobo, Fe/γ-Al_2O_3 and Fe-K/γ-Al_2O_3 as reverse water-gas shift catalysts, Catal. Sci. Technol. 6 (2016) 5267–5279, https://doi.org/10.1039/c5cy02111a.